PCCP

Accepted Manuscript

Journal Name

ARTICLE

An in-situ Surface Electrochemistry Approach towards Whole-cell Studies: Structure and Reactivity of a *Geobacter sulfurreducens* Submonolayer on Electrified Metal/Electrolyte Interfaces

Akiyoshi Kuzume [a*], Ulmas Zhumaev [a], Jianfeng Li [a]†, Yongchun Fu [a], Michael Füeg [a], Marta Estévez [b], Zulema Borjas [b,c], Thomas Wandlowski [a], Abraham Esteve-Nuñez[b,c*]

A direct electron transfer process between bacterial cells of electrogenic species *Geobacter sulfurreducens* (*Gs*) and electrified electrode surfaces was studied to exploit the reactivity of *Gs* submonolayers on gold and silver surfaces. A submonolayer of *Gs* was prepared and studied to explore specifically the heterogeneous electron transfer properties at the bacteria/electrode interface. In-situ microscopic techniques characterised the morphology of the *Gs* submonolayers in the operating condition. In addition, complementary *in-situ* spectroscopic techniques that allowed to access *in-situ* molecular information of the *Gs* with high surface selectivity and sensitivity were employed. The results provided clear evidences that the outermost cytochrome C in *Gs* is responsible for the heterogeneous electron transfer that is in direct contact with the metal electrode. Feasibility of a single cell *in-situ* studies under operating conditions was demonstrated where the combination of surface-electrochemical tools at the nano- and micro-scale with microbiological approaches can offer unique opportunities for the emerging field of electro-microbiology to explore processes and interactions between microorganisms and electrical devices.

1. Introduction

The recent development in electrochemistry has focused predominantly on the characterisation of the solid/liquid interface to understand the electron transfer (ET) reactions and the effect of electrode surface structure on the interfacial reactivity (structure/function correlations) at the molecular level. The interfacial electrochemistry underwent a significant progress by the introduction of well-defined single crystal electrode surfaces as a major breakthrough that led to other new surface technologies such as microscopic and spectroscopic techniques as well as theoretical simulations. *In-situ* scanning tunnelling and atomic force microscopy gave interfacial electrochemistry an atomic/molecular resolution of adsorbates on pure metal electrode surfaces, opening new worlds of microscopic structures and processes. In addition, *in-situ* spectroscopic techniques, such as surface enhanced Raman and infrared spectroscopies, allow monitoring simultaneously the electrochemical reactivity and structural changes of the redox-active species vicinal to the surface. Similar efforts are now visible in interfacial bio-electrochemistry of metalloproteins and DNA-based molecules. The underlying fundamentals of the ET at solid/electrolyte interfaces have been increasingly well understood with the recent bio-electrochemical studies on redox-active metalloproteins. This has further improved the voltammetric sensitivity and the structural interpretation of the bio-electrochemical solid/electrolyte interface down to single molecular levels by utilizing *in-situ* spectroscopic and microscopic techniques which have increased the structural resolution and surface sensitivity under conditions where the bio-molecules are active in their ET function. With the molecular level understanding of the metalloproteins function, the extracellular ET process and the redox activity of the whole bacterial cell can be addressed to explore the function of the single bacterial cell at solid/electrolyte interfaces.

The discovery of the extracellular ET stimulated a wide range of fundamental and applied studies of the microbe/electrode interface with unique technological opportunities in bioenergetics and bioremediation.[1-6] Potter provided as early as 1911 evidence that electrons from microbial metabolisms can be harvested with electrodes.[7] However, only recent findings that certain Iron (III)-reducing bacteria are capable of complete oxidation of organic compounds to carbon dioxide and of efficient ET via direct electrode contact pave the way for the development of microbial fuel cells.[8,9] The highest current densities of known

pure cultures are produced by the Iron (III)-reducing bacteria *Geobacter sulfurreducens* (*Gs*).[1-3,10-12] Genetic and gene expression analysis suggested that electrically conductive pili[13-20] and the outermost c-type cytochrome OmcZ are key components for optimal current production.[1-3,13,14] Interfacial ET between individual bacteria and an electron accepting electrode (anode) is proposed to be dominated by the extracellular c-type cytochrome OmcZ.[1-3] The protein contains eight heme centres with redox potentials ranging between -0.62 V and – 0.26 V (vs. Ag/AgCl). Experiments with gold-labelled antibodies revealed that the OmcZ are located at the outer cell matrix near the electrode surface, and may act as "electrochemical gate" for the ET.[21,22]

Although several studies investigated the behaviour of outer membrane cytochromes (OMC), including OmcZ and OmcS embedded in biofilms of *Gs*, the role of these cytochromes in the interfacial ET is far from being understood. The adaption of electrochemical techniques, such as voltammetry and chronoamperometry, has opened a new approach towards understanding of ET mechanisms and specific interactions of the electricity-producing bacteria *Gs* with electrodes.[10,11,23-25] This research was extended recently by several groups, who combined macroscopic electrochemical measurements with *in-situ* structure-sensitive experiments employing surface-enhanced infrared absorption spectroscopy (SEIRAS),[10,11,27] UV-VIS,[19,28] and Raman spectroscopy[29-31] to explore whole-cell systems in thick biofilms upon polarisation. The simultaneous monitoring of the electrochemical response and the structural changes of these redox-active microorganisms in biofilms is important for unravelling ET processes and complex interactions occurring in a natural and/or engineering environment. However, it is essential that the comprehensive *in-situ* surface studies need to be carried out on the submonolayer of microbial cells, not on the thick biofilms like these reported in literatures,[10,11,19,27-30] to explore the true ET process at bacteria/electrode interface.

In this work, we present unprecedented interfacial electrochemistry study on a submonolayer of *Gs* to explore the initial stages of *Gs* adsorption and the reactivity of the ET process at well-defined electrified metal/electrolyte interfaces. Our strategy combines single crystal electrochemistry with *in-situ* atomic force microscopy (AFM) to characterise the morphology of *Gs* submonolayers, with SEIRAS[32,33] and gap-mode Raman spectroscopy (GM-SERS)[34] to access *in-situ* molecular information of the *Gs*/electrode interfaces with high surface selectivity and sensitivity. We demonstrate that the complementary techniques SEIRAS and GM-SERS, as applied to *in-vivo* studies with *Gs*, allowed monitoring the electrochemical turnover of the oxidized and reduced states of c-type cytochromes of active *Gs* cells directly in contact with the electrode (Scheme 1).

2. Results and discussion

A submonolayer of *Gs* was prepared in well defined condition using the electrostatic adsorption of the bacteria cells, which bear a negative surface charge, on positively charged Au(111) or Ag(111) electrodes in a 50 mM bicarbonate buffer solution containing 20 mM acetate, previously deoxygenated with $N_2:CO_2$ (4:1) (see detail in SI Figure S1). These conditions ensure that *Gs* cells adsorb in their stable oxidized form.[10,11,23,24] Figure 1a displays a typical chronoamperometric transient as monitored for cell immobilisation on Au(111) at E = 0.40 V. The microbial production of current from those cells in direct contact with the electrode is demonstrated clearly. After an initial decrease, the reaction current increases and appears to level off at 2 μAcm^{-2} within the time interval monitored (Note that the fully established biofilm reaches current densities of 0.5 $mAcm^{-2}$ under our experimental conditions, see SI Figure S2). The morphology of the bacterial adlayer as obtained after 12 h polarisation was characterised by scanning electron microscopy (SEM) and *in-situ* AFM (inset Figure 1a and Figure S3). Both confirmed the presence of a submonolayer of rather isolated, homogeneously distributed microbial cells firmly attached to the electrode surface. The average population of *Gs* cells amounts to 10 ± 2 cells per 100 μm^2, which translates into a coverage of ~ 10 %. The formation of the submonolayer ensures that the further *in-situ* investigation focuses only on the ET at the bacteria/electrode interface, and not at the bacteria/bacteria interface.

Non-contact AFM in buffer solution revealed a typical size of individual cells as 1.6 ± 0.3 μm in length, 0.6 ± 0.1 μm in width and an apparent height of 0.4 ± 0.1 μm (See SI Figure S3). The cell surface appeared to be rather smooth, which is distinctly different from AFM data reported for *Shewanella* genus cells in an argon atmosphere.[35]

Complementary structure data on the electrostatic immobilisation of *Gs* were obtained by *in-situ* SEIRAS in a vertical attenuated total reflection configuration (ATR-SEIRAS[31,33]) on quasi-single crystalline Au(111-25nm) films in contact with the bacteria–containing buffer solution. Figure 1b displays a typical set of time-dependent difference spectra recorded in intervals of 20 min at 0.20 V with the single beam spectrum at t = 0 as reference. ATR-SEIRAS probes the whole-cell submonolayer in immediate contact with the conducting gold film up to a penetration depth of 5 nm with high surface sensitivity.[32] The *in-situ* spectra as plotted in Figure 1b reveal several positive and negative going bands representing the accumulation and depletion of species within the interfacial region probed in function of time. The band at 1659 cm^{-1} represents the C=O stretching mode of an amide group. The frequency of this band depends on the secondary structure of the protein backbone. Comparison with literature data[23,24,36-38] leads to the assignment of this band as a representation of the amide I α-helix. The band overlaps with the negative going bending mode of interfacial water, $\delta(H_2O)$ (1630 – 1680 cm^{-1}).[33] The bands at 1565 cm^{-1} and 1309 cm^{-1}, representing the protein-related amide II and amide III modes,[27,37] as well as protein-related bands at 1602, 1531, 1387 and 1254 cm^{-1} incre-
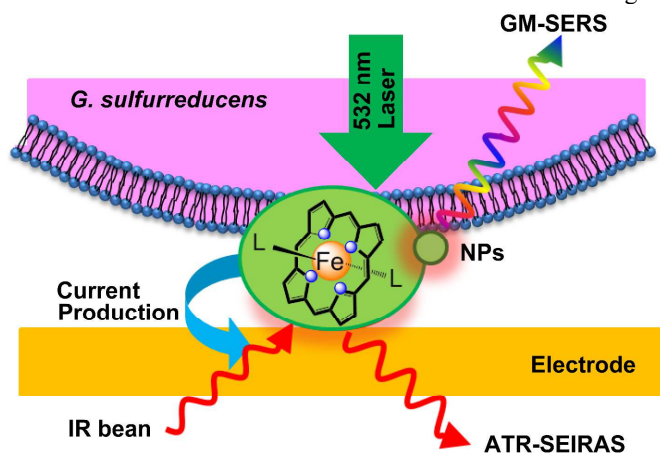
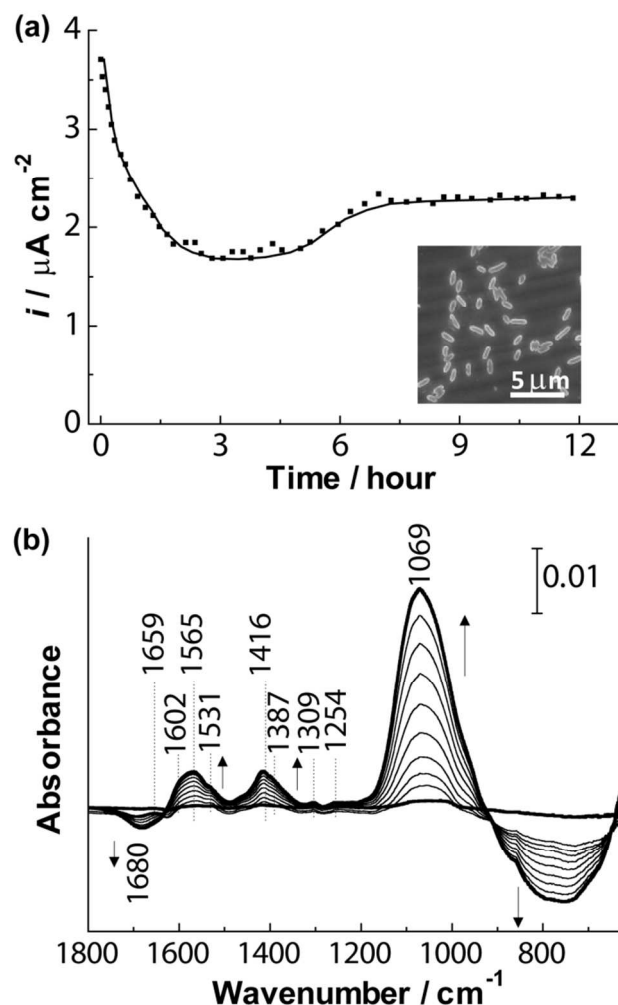**Scheme 1** Representation of the bacteria/electrode interface.

Figure 1. Accumulation of *Gs* (a) Chronoamperometric curve of current production of *Gs* on Au(111) at 0.40 V in the 50 mM bicarbonate buffer solution containing 20 mM acetate in a $N_2:CO_2$ (4:1) atmosphere. Inset typical SEM image of *Gs* after 12h of polarisation. The average coverage of the *Gs* cell was 10 ± 2 cells per 100 μm²; (b) *in-site* ATR-SEIRA spectra recorded during the accumulation process of *Gs* cells on an Au thin film surface at 0.20 V. The reference spectrum was acquired before the addition of *Gs* cells. The single beam spectra were recorded every 20 min after the addition of bacterial cells. The resolution of the spectra is 2 cm⁻¹.

ase in intensity with time,[23,24,37,38] while a broad negative band around 780 cm⁻¹, due to the libration mode of water molecules,[39] decreases in intensity. The increase of the amide- and protein-related bands accompanied with the decrease of the two water bands, indicate an increase of the amount of proteins and as such the accumulation of *Gs* cells by the replacement of interfacial water molecules from the electrode surface during the electrochemical polarisation process. The most prominent band at 1069 cm⁻¹ represents stretching modes of the lipopolysaccharide (LPS) network, which is located on the outermost bacterial surface[40,41] in direct contact with the positively charged gold electrode. Table S1 summarises the assignment of the observed IR-bands. These observations

demonstrate the close distance between the bacterial cells and the gold surface, and underline the specific surface selectivity as well as the high sensitivity of in-situ ATR-SEIRAS as applied to whole-cell studies at electrified microbe/electrode interfaces.

The redox-activity of the immobilised microbial submonolayer of *Gs* cells on Au(111) was investigated by cyclic voltammetry (CV) upon scanning the electrode potential from 0.40 to -0.60 V (Figure 2a). The direct electrochemical detection of the redox signals in the CV shows clearly that some domains of the outermost microbial surface are close enough to the electrode to undergo ET across the interface. The electrochemical response reaches a steady state after five cycles accompanied by a considerable decrease of the redox current in the entire potential region (inset Figure 2a). The corresponding voltammogram is characterised by two pairs of peaks P1/P1´ and P2/P2´ with mid-point potentials at -0.12 V and -0.33 V. The electrochemical behaviour at a steady state with the peak-to-peak separations of 0.21 V and 0.25 V at a scan rate of 0.01 Vs⁻¹ indicate a slow, surface-confined redox process (see SI Figure S4 for detail). We note that these redox potentials are in the same range as those previously reported in the extracellular c-type cytochrome OmcZ.[21,22] We also like to emphasise that the redox current values of the *Gs*-modified surface as obtained during the first CV cycle could be recovered by an additional polarisation at 0.40 V for several hours.

The above interpretation of the CV data is supported by ATR-SEIRA spectra, which were recorded during potential cycling (Figure 2b) as well as by SEM study. The *Gs*-related bands decreased significantly in intensity upon potential cycling, accompanied with the increase in intensity of interfacial water bands. Comparative SEM images recorded after 8 potential cycles revealed that the *Gs* coverage decreased by ca. 80 % to 2 cells per 100 μm². These observations indicate that the microbial cells partially desorbed from the gold surface due to repulsive electrostatic interactions at reduction potentials (The electrode bears a negative effective charge at $E < 0.00$ V, see SI Figure S1) upon the potential cycling, and were replaced by the interfacial water molecules.

Similar as in the CV experiments, a steady state spectroscopic response is reached after five cycles in ATR-SEIRA spectra. The steady state SEIRA spectra showed a reversible, potential-dependent behaviour (see SI Figure S5). Taking the spectrum at 0.20 V, *i.e.* the oxidized form of the surface-confined *Gs* cells, as reference reveals the evolution of the amide I signal at 1686 cm⁻¹ accompanied by an increase in intensity of the interfacial water bending ($\delta(H_2O)$) and stretching ($\nu(OH)$) modes during the cathodic scan. The amide I and water bands decreased during the subsequent anodic scan. These experimental observations reveal the following important aspects: (i) The reversible evolution of the steady state SEIRA spectra upon potential cycling between the reduction and oxidation forms of *Gs* suggests that the coverage of *Gs* does not change any more, although the interfacial response of cells and water change. (ii) The microbial cells retain the direct electrical communication to the metal electrode. (iii) The significant potential-dependent shift of the amide I band from 1659 cm⁻¹ (oxidized state) to 1686 cm⁻¹ (reduced state) suggests a secondary structure change of redox active proteins from α-helix to β-turn.[36,37] The electrical field-induced conformation transition may lead to a more favourable configuration for the interfacial electron exchange.
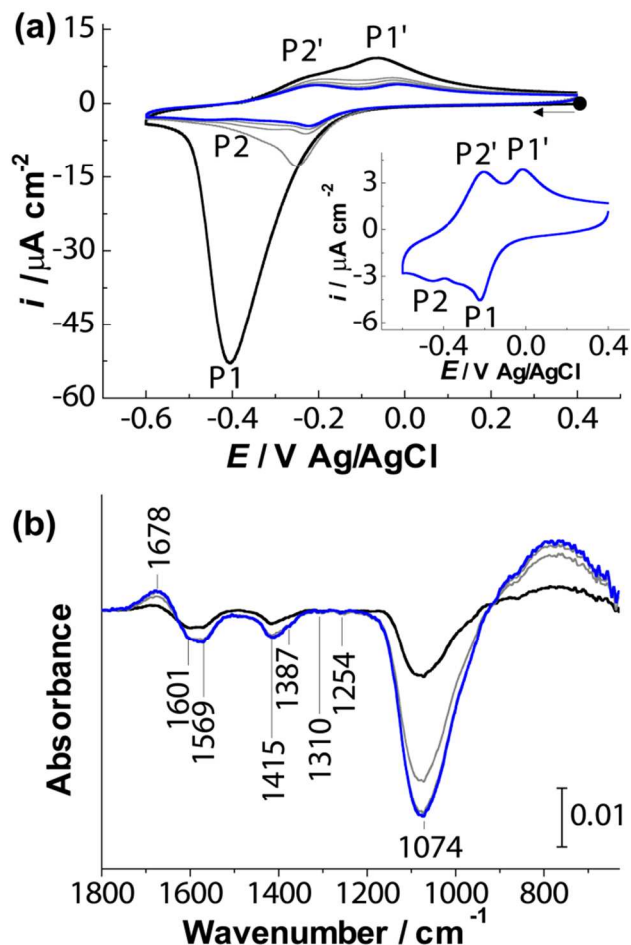
Figure 2. (a) Cyclic voltammograms of *Gs* submonolayer on Au(111) at a scan rate of 0.01 Vs^{-1}. The estimated peak potentials of the redox process are indicated. Black line: cycle 1. Grey lines: cycles two to seven. Inset: CV of the corresponding cycle 8 (blue). (b) A series of ATR-SEIRA spectra of the *Gs* submonolayer acquired at every 0.20 V during potential cycling to monitor the spectral change of *Gs* cells upon potential excursion. The reference spectrum was obtained at 0.20 V before potential cycling.

Structure properties of the heme centres in the outer membrane cytochrome C units, such as OmcZ, are directly accessible during the interfacial ET by *in-situ* gap mode surface-enhanced Raman spectroscopy (GM-SERS). GM-SERS employed 50 to 60 nm in diameter silver nanoparticles (NPs) as plasmonic antennas,[42,43] which are mixed with *Gs* solution and subsequently drop-casted at submonolayer coverage on a smooth Ag(poly) electrode. The SEM analysis of the prepared Raman samples revealed that the mono-disperse silver NPs are deposited as aggregates and are located vicinal to the bacteria cells (see SI Figure S6). The cell population is estimated as 9.4 cells per 100 μm^2, which leads to a 10 % surface coverage. We like to comment on the use of silver NPs deposited on a smooth Ag electrode. This combination enables the choice of a green excitation laser, which tails with the plasmonic resonance of the NPs as well as with the Q-bands of the heme centres. The latter resonance effect cannot be exploited on gold electrodes because the energy of the required red laser is too far off the resonance

states. Finally, we like to stress that the electrochemical behaviour of Ag(poly) and Au(111) electrodes modified with a submonolayer of *Gs* is rather similar to the data reported for the gold electrodes in Figure 2a (SI Figure S7).

The upper spectrum in Figure 3a shows the GM-SERS response of a submonolayer of *Gs* in contact with silver NPs on a smooth Ag(poly) electrode as recorded at $E = 0.00$ V. Although it is difficult to make an unambiguous assignment of individual bands[29] due to the broad features between 1500 and 1650 cm^{-1}, the spectrum reveals several distinguishable bands from c-type cytochromes in the oxidized form by comparing with a normal Raman spectrum of solid *Gs* sample (see SI Figure S8a). These bands and their tentative assignment are summarised in Table S2.[35,44-46] We also monitored the spectra of the bare Ag-NPs in the absence of *Gs*, and did not observe
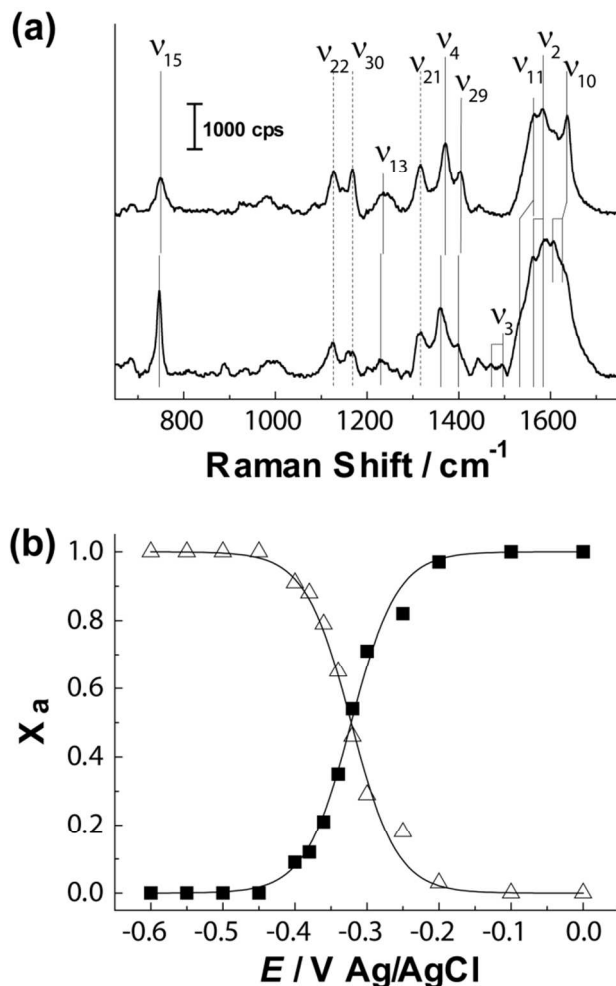

Figure 3. (a) Potential dependent GM-SER spectra of a *Gs* submonolayer mixed with Ag NPs in the oxidised state at 0.00 V (upper) and the reduced state at -0.60 V (lower), respectively. The spectra were obtained with the excitation at λ = 532 nm (laser power at 1 mW with 150 μm defocussed, acquisition time of 10 s); (b) potential dependent molar fraction (X_a) of the oxidized (full square) and the reduced (empty triangle) form derived from the component analysis of the ν_{15} band in the experimental GM-SER spectra. The solid lines represent fits of the Nernst equation for a one-electron redox couple (see detail in text and SI9).

any vibrational features of comparable intensity in 650 cm^{-1} ≤ ν ≤ 1750 cm^{-1} (see SI Figure S8b).

The position of the spin-state marker bands ν$_2$ and ν$_{10}$ indicate a six-coordinated low-spin (LS) state of the heme with a histidine and a methionine group as axial ligands.[44] This result suggests that the OMCs retain mostly their native structure at the positively polarised electrode/electrolyte interface upon constant laser radiation. The observation of a rather strong ν(CC)$_{propionate}$ vibration at 976 cm^{-1} suggests further that the propionate moieties of the heme groups are in close contact with the Ag NPs and/or the silver surface.[41,46,47] Our Raman experiments also demonstrate that the presence of the Ag NPs does not seem to interfere with the active functionality of the surface-confined *Gs* cells, although one cannot exclude a possibility of the partial internalisation of silver NPs. This conclusion is in agreement with observations by Law et al. based on biological reduction experiments with Ag(I) salts.[48]

Potential excursion towards negative values leads to the electrochemical reduction of the *Gs*, which is accompanied by distinct changes in the simultaneously recorded Raman spectra. As an example, the lower spectrum in Figure 3a displays data recorded at E = -0.60 V. We observed a downshift in wavenumber and a splitting of the spin marker states in ν$_2$, ν$_4$, ν$_{10}$, ν$_{11}$ and ν$_{15}$ modes. (Table S2). We also found two new bands at 1494 cm^{-1} and 1470 cm^{-1}, which are assigned to a split spin-marker ν$_3$-mode.[44] The corresponding vibration band in the oxidized state of *Gs* could not be resolved at E = 0.00 V, most probably due to sensitivity limitations of the resonance mode upon excitation with the green laser.

The two strong bands ν$_4$ and ν$_{15}$ are particularly sensitive to the redox state of the heme protein.[35] Both represent symmetric ring breathing modes of the pyrrole moiety, which is N-coordinated to the Fe-center. We analysed quantitatively the integrated intensity of the redox marker band ν$_{15}$ in function of the applied electrode potential to monitor spectroscopically the redox-response of the adsorbed microbial cells since this band is rather isolated from other bands. Figure 3b displays the data of the ν$_{15}$ mode. The integrated intensity of the reduced form (empty triangle) increases in a *s*-shaped form from 0.00 V until saturation is reached at E ≤ -0.45 V. The ν$_{15}$-related band position decreases from 748 to 745 cm^{-1} reaching again a constant value at E ≤ -0.45 V. Simulating this redox process within the *Gs* submonolayer by the superposition of the component spectra, assuming just one oxidized and one reduced form (see detail in SI 9), allows estimating the relative concentrations of the two redox states as a function of the applied electrode potential.[29,44] A fit of the Nernst equation leads to an effective redox potential E_{eff} = -0.32 ± 0.01 V and an effective number of exchanged electrons n_{eff} = 0.8 ± 0.1. The former value is in good agreement with the range of the *Gs*-related redox-potentials as derived from our voltammetric experiments with well-defined gold and silver electrodes (*c.f.* Figure 2a and SI Figure S7). The n_{eff} value is lower than 1, the expected value for the oxidation/reduction of a c-type cytochrome of uniform nature. This result suggests a certain distribution of interfacial redox potentials, which is, again, in agreement with the multiple peak voltammetric profiles. We also like to mention that a similar conclusion was suggested by Millo et al. in a recent resonance Raman experiment with catalytically-active thick microbial biofilms.[29]

As a second important results of our *in-situ* GM-SERS study we point out that the splitting of the spin-marker modes ν$_2$, ν$_3$ and ν$_{10}$ (Figure 3b and Table S2) upon transformation of

the *Gs* submonolayer into the reduced form indicates the coexistence of a low spin (LS) and a high spin (HS) state. The nature of this transition is not yet clear.

3. Experimental

3.1 Microbial inoculums and growth medium

Culture of microorganisms: *Geobacter sulfurreducens* (*Gs*) was anaerobically cultured in a serum bottle using a freshwater medium with 50 mM sodium bicarbonate including minerals and vitamins.[49] Acetate (20 mM) was supplied as a sole carbon source and electron donor while fumarate (40 mM) was used as a sole electron acceptor. The pH of the medium was kept constant at 7.1 by bubbling with an N$_2$+CO$_2$ (4:1) gas mixture through the solution. The mixed gas was filtered through a Varian CP17970 oxygen filter to avoid oxygen traces.

Biofilm formation: 10 mL of a *Gs* culture at exponential phase (OD$_{600}$ = 0.3) was inoculated into a sealed electrochemical cell filled with deaerated buffer solution (100 mL) supplied with 20 mM sodium acetate, minerals and vitamins. The anaerobic condition was maintained by flowing a mixture of N$_2$:CO$_2$ (4:1) through the upper space of the electrochemical cell. A constant potential of 0.40 V vs. Ag/AgCl was applied to the Au working electrode using a potentiostat (μAutolab® system, The Netherlands) to monitor the current production and the formation of the biofilm. A peristaltic pump was switched on 24 hours after the inoculation and used to supply fresh growing media with a dilution rate of 0.06 h^{-1}. The temperature was controlled at 33.0 ± 0.3 °C throughout the biofilm experiments.

3.2 Preparation of Ag nanoparticles (NPs)

Citrate-stabilized Ag NPs with a mean diameter of 80 nm were synthesised by reducing 200 mL of a boiling 0.018 wt% AgNO$_3$ solution with 4 mL of 1 wt% sodium citrate. A colour change from yellow to pale green took place within 20 sec. The solution was kept boiling for 4 h, and was then stirred until cooling down to room temperature.[50] 1.5 mL of the NP solution was subsequently cleaned and concentrated by a factor of 100 via centrifugation (5500 rpm for 15 min, 3 times), which led to 10-20 μL of a dark green sediment. This sediment was mixed with concentrated *Gs* and subsequently casted and dried on a flat Ag (or Au) electrode in an Ar atmosphere. The electrode was inserted into a home-made Raman cell, which was filled in a next step under potential control with deaerated buffer solution.

3.3 Electrochemistry

The electrochemical studies were performed in a custom-made electrochemical glass cell equipped with a Pt counter electrode and an Ag/AgCl (saturated KCl) reference electrode. All potentials given in this paper refer to this reference electrode. The Au(111) bead electrode, used as a working electrodes, was flame-annealed before each experiment and quenched gently with MilliQ water.

3.4 Electrochemical attenuated total reflection surface enhanced infrared absorption spectroscopy (EC-ATR-SEIRAS)

ATR-SEIRAS was carried out in a vertical home-made glass cell equipped with a Pt wire and an Ag/AgCl (saturated KCl) electrode as counter and reference electrodes in a Kretschmann ATR-configuration at room temperature (20 °C).[33] A thin Au film (30 nm thickness) was vapour-deposited onto the flat surface of a ZnSe hemisphere prism. The IR beam was focused onto the electrode/electrolyte interface by passing through the back of the hemispherical ZnSe prism. The incident angle was typically 70° as referred to the surface normal. The IR radiation, totally reflected at the interface, was measured with a liquid-nitrogen cooled MCT detector (Model MCT D316/6) using a Bruker Vertex80 spectrometer. The spectra were collected with p-polarised light with a resolution of 2 cm^{-1}. The resulting spectra are plotted in absorbance units defined as $A = -\log(R_s/R_{ref})$, where R_s and R_{ref} are the reflectance values of the single beam spectra at the sample and at the reference potential, respectively. The SEIRAS experiments were performed using a sodium bicarbonate solution (50 mM) containing sodium acetate (20 mM), which was equilibrated at pH 7.1 upon purging with a N_2+CO_2 (4:1) gaseous mixture.

3.5 Electrochemical gap-mode surface enhanced Raman spectroscopy (EC-GP-SERS)

In-situ GM-SERS measurements were performed with a LabRAM HR800 confocal Raman microscope (Horiba Jobin Yvon). The excitation wavelength was 532 nm (Nd:YAG laser). The power of the laser on the sample was 1 mW, and a 50 times magnification long-working-distance objective (8mm) with a numerical aperture of 0.1 was used to focus the laser onto the sample to collect the scattered light in a backscattering geometry. The custom-made spectro-electrochemical flow cell was equipped with a Pt wire and an Ag/AgCl (saturated KCl) electrode serving as a counter and reference electrodes, respectively. The GM-SERS experiments were performed in a buffer solution (50 mM sodium bicarbonate + 20 mM sodium acetate) under continuous bubbling of a mixture of N_2+CO_2 (4:1) to deaerate the solution, as well as to keep the pH at 7.1.
Ag nanoparticles were mixed with concentrated Gs (5000 rpm for 4 min, 3 times), casted and dried on an Ag electrode surface in an Ar atmosphere. The electrode was mounted into the home-made Raman cell, which was subsequently filled with deaerated buffer solution, followed by a continuous polarisation at 0.00 V for 12 h before acquiring spectra.

3.6 Atomic force microscopy

A cell suspension of Gs was diluted (1:6) in 50 mM bicarbonate buffer solution containing 20 mM sodium acetate and incubated in a electrochemical glass cell under continuous bubbling with a N_2+CO_2 (4:1) mixture. A Gs submonolayer was first formed on an Au electrode by polarising 12 h at 0.40 V (Ag/AgCl). Subsequently, the submonolayer was treated with a 2% glutaraldehyde solution for 15 s and then rinsed gently with bicarbonate buffer solution. The AFM measurements were performed in non-contact mode using a *NanoSurf easyScan2* SPM system with PPP-NCSTAu-10 cantilevers (Nanosensors, spring constant 9.8 Nm^{-1}). Data analysis was carried out using the WSxM software.[51]

3.7 Scanning electron microscopy

The coverage of the microbial submonolayer samples were examined with a HITACHI S-3000N Scanning Electron Microscopy operated at 25 kV, equipped with an Energy dispersive X-ray Spectroscopy (EDX) (Noran SIX NSS200) system allowing local chemical composition analysis. A Gs submonolayer was prepared in the same way as the AFM measurement, followed by the sputtering with gold for the observation by SEM.

4. Conclusions

The electrochemical and spectroelectrochemical experiments of submonolayers of *Geobacter sulfurreducens* on well-defined gold (and silver) electrode/electrolyte interfaces revealed that the direct ET took place between the microbial cells and the electrified surface through c-type cytochromes embedded into the outer membrane. The suggested potential ranges of the OMCs from spectral data are in good agreement with the redox processes as observed in the voltammetric experiments. Considering the submonolayer coverage of rather isolated Gs cells, as demonstrated in our *in-situ* AFM and SEM characterisation studies, and referring to the immunogold-labelling experiments of Inoue et al.,[21,22] we propose that the c-type cytochrome signatures as observed in the present study originate from OmcZ, the redox-active protein, which is assumed to dominate the short-range ET between bacteria cells and the electrified metal electrode. Contributions due to OmcS can be excluded due to the lack of pili in the Gs submonolayer, which represents just the initial stage (< 1 μm thickness) of the several tenth of micrometer typically found in a thick biofilm.[52-55] Furthermore, *in-situ* SEIRAS and GM-SERS provide complementary spectral signatures of structure changes during the oxidation/reduction process of the microorganisms. Our surface-electrochemistry based approach on the submonolayer of microbial cells demonstrate the feasibility on exploring the single cell *in-situ* investigation under operating conditions, but also points out the need of reference experiments with structurally well-defined OMCs for complementary experiments to interpret the electrochemical response of Gs whole cells in more detail. On the other hand, we could clearly demonstrate that the combination of surface electrochemical tools at the nano- and micro-scale with microbiological approaches offers unique opportunities for the emerging field of electromicrobiology,[1-3] to explore processes and interactions between microorganisms and "electrical devices".

Notes and references
[a] Department of Chemistry and Biochemistry, University of Bern, Freiestrasse 3, 3012 Bern, Switzerland. E-mail: Akiyoshi.kuzume@dcb.unibe.ch
[b] Department of Chemical Engineering, University of Alcalá, 28871 Alcalá de Henares, Madrid, Spain. E-mail: Abraham.esteve@uah.es

c IMDEA WATER, Parque Tecnológico de Alcalá, 28871 Alcalá de Heranes, Madrid, Spain.

† Current address: Jianfeng Li: College of Chemistry and Chemical Engineering, Xiamen University, Xiamen, 361005, China

1. D.R. Lovley, *Annu. Rev. Microbiol.* 2012, **66**, 391-409.
2. D.R. Lovley, *Energy Environ. Sci.* 2011, **4**, 4896-4906.
3. D.R. Lovley, *Curr. Opinion Biotech.* 2008, **19**, 564-571.
4. B.E. Logan, *Nat. Rev. Micro.* 2009, **7**, 375-381.
5. K. Rabaey, R.A. Rozendal, *Nat. Rev. Micro.* 2010, **8**, 706-716.
6. U. Schröder, *J. Solid State Electrochemistry* 2011, **15**, 1481-1485.
7. M.C. Potter, *Proc. R. Soc. Lon. B* 1911, **84**, 260-276.
8. D.R. Bond, D.E. Holmes, L.M. Tender, D.R. Lovley, *Science* 2002, **295**, 483-485.
9. D.R. Bond, D.R. Lovley, *Appl. Environ. Microbiol.* 2003, **69**, 1548-1555.
10. H. Yi, K.P. Nevin, B.C. Kim, A.E. Fanks, A. Klimes, L.M. Tender, D.R. Lovley, *Biosens. Bioelectronics* 2009, **24**, 3498-3503.
11. K.P. Nevin, H. Richter, S.F. Covalla, J.P. Johnson, T.L. Woodard, A.L. Orloff, H. Jia, M. Zhang, D.R. Lovley, *Environ. Microbiol.* 2008, **10**, 2505-2514.
12. G.D. Schrott, M.V. Ordoñez, L. Robuschi, J.P. Busalmen, *ChemSusChem,* 2014, **7**, 598-603.
13. J.P. Busalmen, A. Esteve-Núñez, A. Berná, J.M. Feliu, *Angew. Chem. Int. Ed.* 2008, **47**, 4874-4877.
14. J.P. Busalmen, A. Esteve-Núñez, A. Berná, J.M. Feliu, *Bioelectrochem.* 2010, **78**, 25-29.
15. G. Reguera, K.P. Nevin, J.S. Nicoll, S.F. Covalla, T.L. Woodard, D.R. Lovley, *Appl. Environ. Microbiol.* 2006, **72**, 7345-7348.
16. V. Leang, X. Qian, T. Mester, D.R. Lovley, *Appl. Environ. Microbiol.* 2010, **76**, 4080-4084.
17. N.S. Malvankar, M. Vargas, K.P. Nevin, A.E. Franks, C. Leang, B.C. Kim, K. Inoue, T. Mester, S.F. Covalla, J.P. Johnson, M. Rotello, M.T. Tuominen, D.R. Lovley, *Nat. Nanotechnol.* 2011, **6**, 573-579.
18. Y. Qian, PhD Thesis, University of Massachusetts, Amherst, 2009.
19. Y. Liu, H. Kim, R.R. Franklin, D.R. Bond, *ChemPhyChem* 2011, **12**, 2235-2241.
20. S.M. Strycharz-Glaven, R.M. Snider, A. Guiseppi-Elie, L.M. Tender, *Energy Environ. Sci.* 2011, **4**, 4366-4379.
21. K. Inoue, X. Qian, L. Morgado, B.C. Kim, T. Mester, M. Izallalen, C.A. Salgueiro, D.R. Lovley, *Appl. Environ. Microbiol.* 2010, **76**, 3999-4007.
22. K. Inoue, C. Leang, A.E. Franks, T.L. Woodard, K.P. Nevin, D.R. Lovley, *Environ. Microbiol. Reports* 2011, **3**, 211-217.
23. K. Fricke, F. Harnisch, U. Schröder, *Energy Environ. Sci.* 2008, **1**, 144-147.
24. E. Marsili, J. Sun, D.R. Bond, *Electroanalysis* 2010, **22**, 865-874.
25. G.D. Schrott, P.S. Bonanni, L. Robuschi, A. Esteve-Nuñez, J.P. Busalmen, *Electrochim. Acta* 2011, **56**, 10791-10795.
26. J.P. Busalmen, A. Esteve-Nuñez, J.M. Feliu, *Environ. Sci. Technol.* 2008, **42**, 2445-2450.
27. A. Esteve-Núñez, J.P. Busalmen, A. Berná, C. Gutiérrez-Garrán, J.M. Feliu, *Energy Environ. Sci.* 2011, **4**, 2066-2069.
28. R. Nakamura, K. Ishii, K. Hashimoto, *Angew. Chem. Int. Ed.* 2009, **48**, 1606-1608.
29. D. Millo, F. Harnisch, S.A. Patil, H.K. Ly, U. Schröder, P. Hildebrandt, *Angew. Chem. Int. Ed.* 2011, **50**, 2625-2627.
30. B. Virdis, F. Harnisch, D.J. Batstone, K. Rabaey, B.C. Donose, *Energy Environ. Sci.* 2012, **5**, 7017-7024.
31. A. Kuzume, U. Zhumaev, J.F. Li, Y.C. Fu, M. Füeg, A. Esteve-Nuñez, Th. Wandlowski, *Electrochim. Acta*, 2013, **112**, 933-942.
32. M. Osawa, *Bull. Chem. Soc. Jpn.* 1997, **70**, 2861-2880.
33. Th. Wandlowski, K. Ataka, S. Pronkin, D. Diesing, *Electrochim. Acta* 2004, **49**, 1233-1247.
34. L. Cui, B. Liu, D. Vonlanthen, M. Mayor, Y. Fu, J.F. Li, Th. Wandlowski, *J. Am. Chem. Soc.* 2011, **133**, 7332-7335.
35. V. Biju, D. Pan, Y.V. Gorby, J. Fredrickson, J. McLean,; D. Saffarini, H.P. Lu, *Langmuir* 2007, **23**, 1333-1338.
36. A. Barth, *Biochim. Biophy. Acta* 2007, **1767**, 1073-1101.
37. K. Ataka, J. Heberle, *J. Am. Chem. Soc.* 2004, **126**, 9445-9457.
38. L. Marboutin, A. Boussac, C. Berthomieu, *J. Biol. Inorg. Chem.* 2006, **11**, 811-823.
39. N. Nakamoto, in *Infrared and Raman Spectra of Inorganic and Coordination Compounds*, Wiley, New York, 1991, p. 253.
40. J.P. Busalmen, A. Berná, J.M. Feliu, *Langmuir* 2007, **23**, 6459-6466.
41. J.B. Rollefson, C.S. Stephen, M. Tien, D.R. Bond, *J. Bacteriol.* 2011, **193**, 1023-1033.
42. J. Zheng, Y. Zhou, X. Li, Y. Ji, T. Lu, R. Gu, *Langmuir* 2003, **19**, 632-636.
43. R.A. Alvarez-Puebla, R.F. Aroca, *Anal. Chem.* 2009, **81**, 2280-2285.
44. S. Oellerich, H. Wackerbarth, P. Hildebrandt, *J. Phys. Chem. B* 2002, **106**, 6566-6580.
45. L.H. Eng, V. Schlegel, D.L. Wang, H.Y. Neujahr, M.T. Stankovich, T. Cotton, *Langmuir* 1996, **12**, 3055-3059.
46. B.-S. Yeo, S. Mädler, Th. Schmid. W. Zhang, R. Zenobi, *J. Phys. Chem. C* 2008, **112**, 4867-4873.
47. P. Hildebrandt, M. Stockburger, *J. Phys. Chem.* 1986, **90**, 6017-6024.
48. N. Law, S. Ansari, F.R. Livens, J.C. Renshaw, J.R. Lloyd, *Appl. Environ. Microbiol.* 2008, **74**, 7090-7093.
49. A. Esteve-Núñez, M. Rothermich, M. Sharma, D.R. Lovley, *Environ. Microbiol.* 2005, **7**, 641-648.
50. P.C. Lee, D. Meisei, *J. Phys. Chem.* 1982, **86**, 3391-3395.
51. I. Horcas, R. Fernandez, J.M. Gomez-Rodriguez, J. Colchero, J. Gomez-Herrero, A.M. Baro, *Rev. Sci. Instrum*. 2007, **78**, 013705.
52. J.A. Smith, P.-L. Tremblay, P.M. Shrestha, O.L. Snoeyenbos-West, A.E. Franks, K.P. Nevin, D.R. Lovley, *Appl. Environ. Microbiol*. 2014, **80**, 4331-4340.
53. N.S. Malvankar, D.R. Lovley, *Curr. Opinion Biotech*. 2014, **27**, 88-95.
54. X. Liu, P.-L. Tremblay, N.S. Malvankar, K.P. Nevin, D.R. Lovley, *Appl. Environ. Microbiol.* 2014, **80**, 1219-1224.
55. P.S. Bonanni, D. Massazza, J. P. Busalmen, *Phys. Chem. Chem. Phys*. 2013, **15**, 10300-10306.